

Article

Sol-Gel Synthesized Nickel-Oxide-Based Fabrication of Arsenic (As^{3+}) Sensor

Ali Alsalmeh , Huda Alsaeedi , Malak Faisal Altowairqi, Rais Ahmad Khan , Ghadah M. Alharbi and Afnan A. Alhamed

Department of Chemistry, College of Science, King Saud University, Riyadh 11451, Saudi Arabia

* Correspondence: aalsalme@ksu.edu.sa

Abstract: Heavy metal ions can have a negative impact on human health when they are present in the environment and diet. In order to enhance healthcare globally, simple, dependable, sensitive, rapid, and accurate technologies for their detection must be created. Herein, we report a sol-gel preparation of nickel oxide (NiO) nanoparticles. The prepared NiO nanoparticles are extensively characterized by PXRD, SEM, and EDS approaches. The obtained SEM results showed that NiO has a nanosphere-shaped surface morphology. The surface area of a gold electrode (Au) was fabricated with NiO nanoparticles via the drop-casting method. The fabricated electrode with NiO nanoparticles (NiO/Au) was applied as an arsenic sensor. The NiO/Au exhibits decent sensitivity of $3.10 \mu\text{A/ppb}$ and a limit of detection of 1.94 ppb. The NiO/Au also shows good sensing performance for arsenic detection, which includes good stability, repeatability, and selectivity. So far, this is the first report which adopted two electrochemical techniques (cyclic voltammetry and linear sweep voltammetry) for the detection of arsenic using NiO/Au.

Keywords: NiO; sol-gel method; arsenic; sensor



Citation: Alsalmeh, A.; Alsaeedi, H.; Altowairqi, M.F.; Khan, R.A.; Alharbi, G.M.; Alhamed, A.A. Sol-Gel Synthesized Nickel-Oxide-Based Fabrication of Arsenic (As^{3+}) Sensor. *Inorganics* **2023**, *11*, 83. <https://doi.org/10.3390/inorganics11020083>

Academic Editor: Antonino Gulino

Received: 6 December 2022

Revised: 13 February 2023

Accepted: 13 February 2023

Published: 16 February 2023



Copyright: © 2023 by the authors. Licensee MDPI, Basel, Switzerland. This article is an open access article distributed under the terms and conditions of the Creative Commons Attribution (CC BY) license (<https://creativecommons.org/licenses/by/4.0/>).

1. Introduction

Due to the rapid growth of the economy, the environmental issues and energy crisis have become increasingly more prominent [1–4]. Heavy metal ions are listed as top environmental health hazards due to their high toxicity. Both geological and man-made processes are the sources of these heavy metal ions [5–9]. Heavy metal ions can interact with DNA at very low levels, which can result in mutations [10–14]. Therefore, obtaining portable, straightforward, dependable, and effective technology capable of detecting impurities is necessary to support the upkeep of clean and safe drinking water (especially by detecting heavy metal contaminants) [15–20]. Researchers have developed reliable electrochemical sensors with greater sensitivity towards heavy metals using tiny devices based on nano-engineering [20].

Electrochemical techniques and nanomaterials have been combined to create sensors with increased sensitivity, specificity, detection limits, and resilience [21]. An important field of research is the quantitative, ultrasensitive, and ultra-specific detection of heavy metal ions, which can help people access their fundamental right to safe drinking water and better healthcare facilities [22]. Biomolecules have become crucial components for assessing metal ions, including DNA, enzymes, antibodies, and microbes [19]. However, because of their instability and/or difficult handling practices, animals frequently suffer [18]. Due to their unique features, nanomaterials have become excellent alternatives for creating novel sensing platforms [14].

Inorganic arsenic compounds are one of the worst environmental concerns in the world due to their extreme toxicity and lack of biodegradability [15]. Groundwater, the wood-processing sector, fertilizers, the mining industry, herbicides, and the metal electroplating industry are common sources of arsenic [16]. Due to concerns about its toxicity,

arsenic must be detected using selective and extremely sensitive platforms [17]. Due to hydrogeological events, geochemical conditions, and anthropogenic activity, excessively high arsenic concentrations have been found in water supplies [13]. This has had a negative impact on populations in more than 70 regions, including Bangladesh, India, Hungary, China, and the United States. The earth's crust and groundwater both contain arsenic, one of the most poisonous and cancer-causing metals [12]. Atherosclerosis, hyperkeratosis, skin cancer, and irregular heartbeat are just a few of the major health problems that are thought to be induced by long-term exposure to arsenic-tainted water.

In particular, As (III) is the most detrimental oxidation state of arsenic for ecological systems [22]. Regular use of arsenic-contaminated water is likely to result in serious health issues for people, including lung and skin cancer as well as disorders of the heart, neurological system, gastrointestinal system, kidney, and liver [23]. The allowed detection limit of As (III) in drinking water is less than 10 ppb. The main mechanisms of heavy metal toxicity include enzyme inhibition, oxidative stress, and decreased antioxidant metabolism [11]. Free radicals produced by heavy metal toxicity lead to DNA damage, lipid peroxidation, and protein sulfhydryl depletion [18].

Arsenic has been detected selectively and sensitively using a variety of approaches, including inductively coupled plasma mass spectrometry (ICP-MS), X-ray fluorescence (XRF), atomic absorption spectroscopy (AAS), and electrochemical and colorimetric methods [23]. Although these methods are efficient, there are some restrictions on the skill and caution required to use them [24]. AAS, ICP-MS, and neutron activation analysis, for instance, can produce extremely accurate and sensitive data; nevertheless, these techniques are expensive and demand educated staff and competent interpretation (e.g., identifying the occurrence of spectral interferences) [25]. In contrast, colorimetric assays result in arsine gas and are prone to producing false positive/negative results. The detection limitations of polarography techniques are inadequate. Biomolecules must be immobilized on the electrode surface for electrochemical methods to work. Other requirements include expert handling, ideal temperature and pH settings, appropriate storage, etc. In addition, various metal ions can quickly block DNA and enzymes [24].

The conventional techniques are expensive in terms of instrumentation. In addition, these conventional techniques require a sophisticated and large area for installation. An expert is also required for the handling of the sample for investigation purposes. Due to the limitations of the currently used conventional techniques, robust, selective, rapid, ultrasensitive, and simple arsenic detection methods are required.

Each metal has a unique electrode potential, making it a good option for electrochemical detection. Nanomaterials are advantageous due to their high adsorption capacity, simplicity in synthesis, improved catalytic properties, biocompatibility, and superior electrochemical response; these attributes all make them suitable for electron mediators/electrocatalysts for the electrochemical sensing of analytes [26–30]. Electrochemistry-based sensors exhibit excellent sensitivity and selectivity, which makes them suitable candidates for real-time applications [31–33]. Because of their exceptional and distinctive physiochemical characteristics, transition metal oxides (TMOs) have attracted a lot of attention in recent years [24]. Nanostructured TMOs with good surface area, outstanding thermal stability, and optoelectronic features include manganese oxide (MnO_2), zinc oxide (ZnO), cobalt oxide (Co_3O_4), nickel oxide (NiO), copper oxide (CuO), and tin oxide (SnO_2) [25]. Particularly, NiO has been widely investigated in numerous optoelectronic applications, including electrochemical sensors, solar cells, batteries, dye degradation, gas sensors, super-capacitors, and catalysis [34–36]. The use of NiO as an effective electrode material for electrochemical sensing applications was also previously widespread. According to the available literature, NiO has the potential to be used in the construction of glucose, urea, venlafaxine, lactic acid, and endosulfan electrochemical sensors [37–41].

The sol-gel method is time-consuming but has many advantages, such as high chemical reactivity of the precursor due to the process in the solution phase, ability to control the chemical composition, synthesis of uniform compounds, very high production effi-

ciency, and simplicity of the process. In the present study, our group has obtained NiO nanoparticles using the sol-gel approach. Furthermore, a gold electrode (GE) has been modified with the obtained NiO nanoparticles and adopted as an arsenic sensor. Although a gold electrode is expensive, it has excellent electro-catalytic properties. Moreover, a very small area (3 mm) is used as the gold electrode. Electrochemical methods also have some disadvantages, such as short or limited shelf-life, etc., but these can be neglected due to the fast sensing response of electrochemical methods. The constructed arsenic sensor demonstrated good selectivity, limit of detection, and sensitivity, as well as repeatability/stability. So far, no report is available on the use of a NiO-modified GE as an arsenic sensor. To our knowledge, this is the first report which demonstrates the electro-catalytic nature of NiO-GE for arsenic detection with two electrochemical techniques.

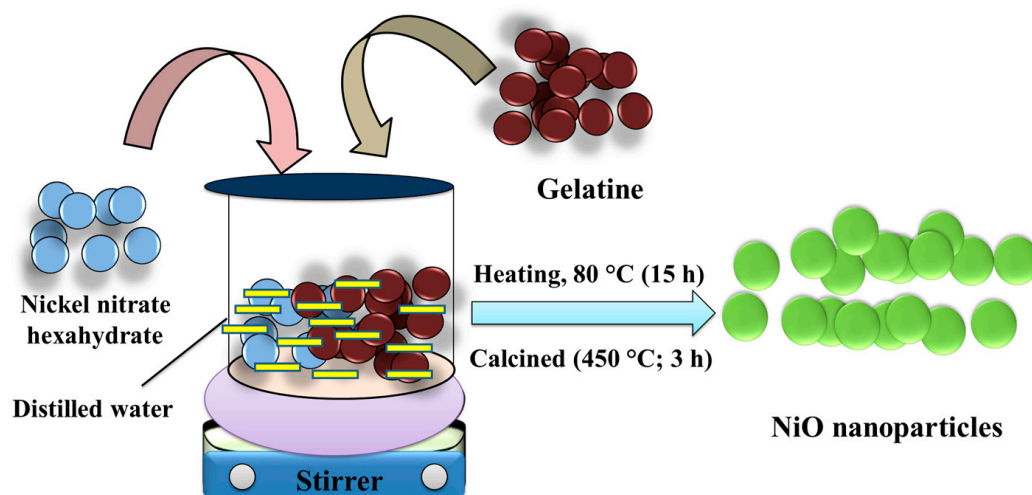
2. Materials and Methods

2.1. Chemicals and Reagents

Nickel nitrate hexahydrate was purchased from Acros. Phosphate-buffered saline (PBS) solutions were purchased from Merck. Nafion (5 wt% in lower aliphatic alcohols and water) was purchased from Sigma-Aldrich (St. Louis, MO, USA). Other chemicals were purchased from TCI and Alfa-Aesar and used without any purification. Gelatin (type: bovine skin) was obtained from Sigma-Aldrich.

2.2. Synthesis of NiO Nanoparticles

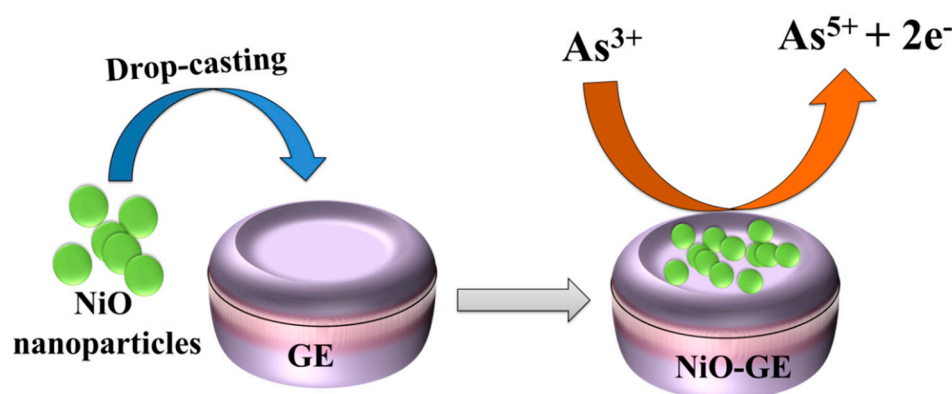
NiO was obtained by adopting the sol-gel preparation method [42]. Briefly, 4.8 g of nickel nitrate hexahydrate was dissolved in 20 mL deionized (D.I.) water with stirring for 0.5 h. Then, 1.9 g of gelatin was prepared in 35 mL of D.I. water with the help of stirring for 0.5 h at 55–60 °C. This stirring at 55–60 °C yielded a clear solution of gelatin. The nickel nitrate hexahydrate solution was slowly added to the gelatin solution and heated at 80 °C using a water bath with continuous stirring for 15 h (Scheme 1). The bright green gel-like viscous product obtained was calcinated at 450 °C for 3 h, which yielded NiO nanoparticles.



Scheme 1. Schematic picture for sol-gel preparation of NiO.

2.3. Fabrication of the Glassy Carbon Electrode

The electrode (GE) surface was cleaned using 0.5 μm alumina slurry and velvet pad and was further modified with the obtained NiO. In brief, NiO ink was obtained by dispersing 3 mg of NiO in 2 mL of ethanol, and nafion was added as a binder. The dispersion was sonicated for 0.5–1 h. Later, 9.5 μL of the obtained NiO ink was transferred onto the active 3 mm surface of the GE via the drop-casting method. This modified electrode (NiO-GE) was dry under the natural air condition and used as an arsenic sensor (Scheme 2).



Scheme 2. Schematic representation for the preparation of NiO-GE.

2.4. Instrumental

This study used a RINT 2500 V X-ray diffractometer with Cu K irradiation ($\lambda = 1.5406$) to perform a powder X-ray diffraction pattern (PXRD) of the obtained NiO with scan step size of 0.02° . The elemental composition of SnO₂ was evaluated using an Energy Dispersive X-ray (EDX) spectroscope (Oxford Instrument' X-max, Aztec, Abingdon, Oxfordshire, UK), while the structural morphology of NiO was acquired using a Supra 55 Zeiss-Field-Emission Scanning Electron microscope (FE-SEM). The NiO powder sample was deposited on carbon tape and a platinum layer was coated on the NiO powder sample for taking FE-SEM images. The magnification for the FE-SEM images was 80,000 at 10 keV. The Bio-Rad FTS 300 MX was used to carry out the Fourier-transform infrared spectroscopy (FTIR) investigation. A CH potentiostat instrument with a three-electrode system (GE acts as the working electrode, silver/silver chloride (Ag/AgCl) serves as the reference electrode, and platinum wire serves as the counter electrode) was used for the determination of As³⁺ using cyclic voltammetry and linear sweep voltammetry techniques.

3. Results and Discussion

3.1. Physicochemical Characterization

The structure, phase composition, and purity of NiO was determined by powder X-ray diffraction (PXRD). Figure 1a depicts the obtained PXRD pattern of the obtained NiO. The PXRD pattern shows the appearance of major diffraction peaks at 37.63 , 43.55 , 63.12 , 75.75 , and 79.55° . These diffraction peaks indicate the presence of (111), (200), (220), (311), and (220) diffraction planes (Figure 1a). This PXRD spectrum of NiO is consistent with JCPDS number of 01-78-0423. The crystallite size of the NiO was determined by using the Debye–Scherrer equation, which is given below.

$$\text{Crystalline size (D)} = (k\lambda/\beta\cos\theta) \quad (1)$$

where k = Scherer's constant (0.94), λ = wavelength (1.54178 \AA), and β = width at half maximum (FWHM).

The crystallite size of the NiO was found to be $\sim 39.8 \text{ nm}$. In addition, no peaks for impurity were observed in the PXRD pattern. Hence, it was concluded that NiO was obtained with good phase purity.

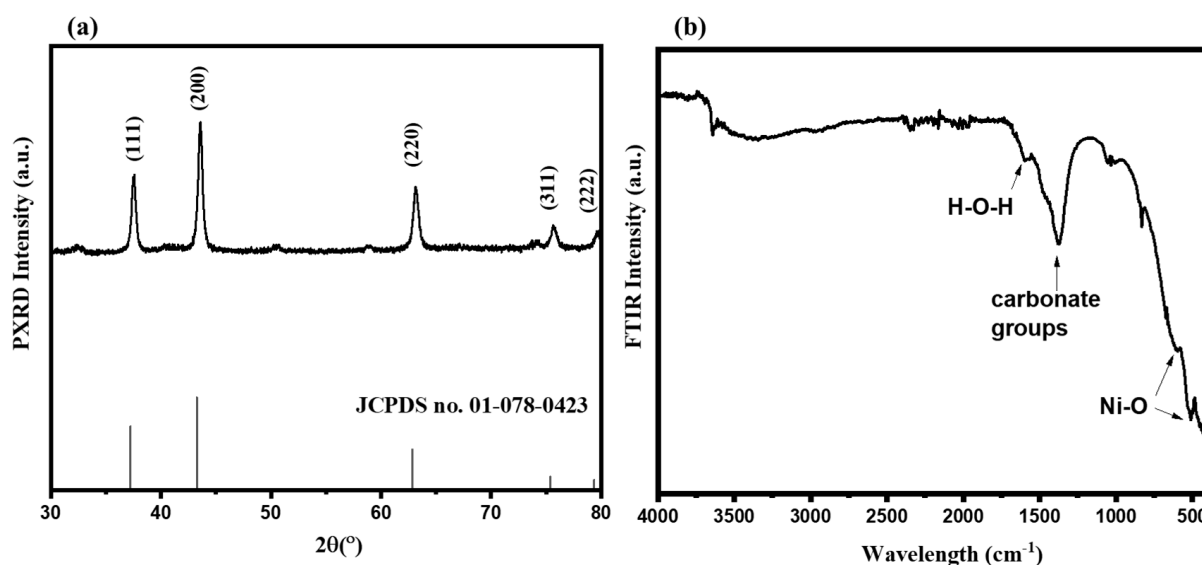


Figure 1. (a) PXRD pattern and (b) FTIR of NiO.

The FTIR is a significant tool to further verify the formation of NiO. In this regard, the FTIR spectrum of NiO was obtained in the wavelength range of 4000–400 cm^{-1} . The FTIR spectrum of NiO is shown in Figure 1b. The FTIR spectrum of NiO shows two vibration bands at 512.4 cm^{-1} and 608.47 cm^{-1} , which indicate the Ni-O bonds in the finger-print region (Figure 1b). The band at 1386 cm^{-1} can be assigned to the carbonate groups which may arise due to the CO_2 in the air. The appearance of the band at 1598 cm^{-1} may be assigned to the H-O-H bending vibration mode. The obtained FTIR data are consistent with previous reports [43–45]. The particle structural morphology has the potential to play a significant role in optoelectronic and electrochemical devices or applications. For this connection, it would be better to study the structural morphological property of the obtained NiO.

The FE-SEM images were captured on the microscope, and the obtained FE-SEM pictures are displayed in Figure 2a,b. The FE-SEM results indicated the presence of agglomerated NiO nanoparticles. These NiO nanoparticles were interconnected with agglomeration. Most of the NiO nanoparticles are present in the range of 50–80 nm.

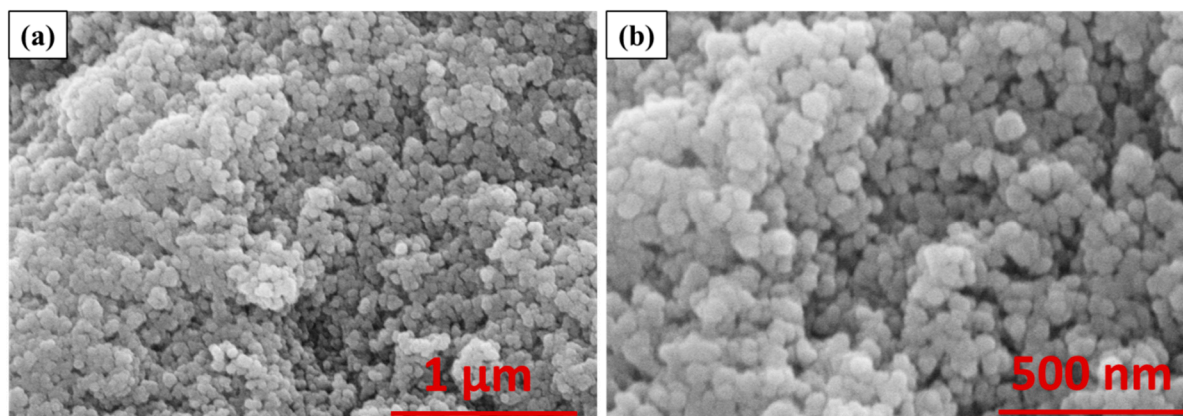


Figure 2. (a,b) FE-SEM images of NiO.

Thus, it is clear that NiO nanoparticles are formed via the sol-gel approach (Figure 2a,b). The agglomeration of some NiO nanoparticles can be seen in Figure 2b because some NiO nanoparticles may be present with loose joints. To further clarify the statement that NiO has been formed with good phase purity, we used EDS spectroscopy to investigate the

elemental composition of the obtained NiO nanoparticles. The EDS spectrum of NiO exhibits the peaks related to the Ni and O elements and confirmed that NiO has been formed with decent phase purity (Figure 3). The Ni and O were present with atomic percentages of 77.21% and 22.79%, respectively.

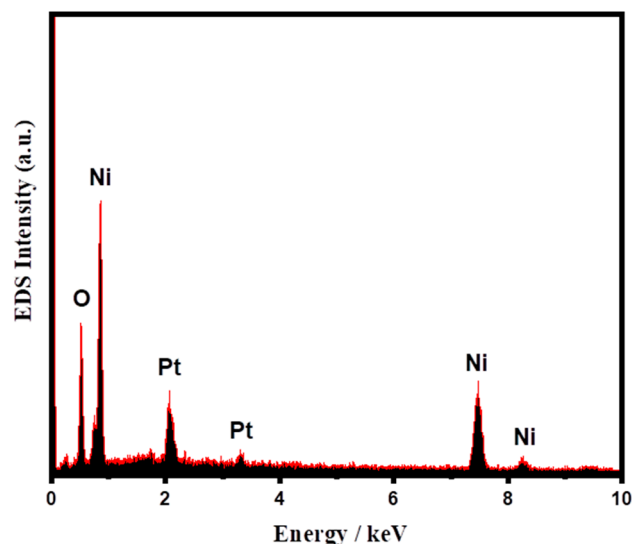


Figure 3. EDS spectrum of NiO.

3.2. Electrochemical Study of Arsenic Sensor

The cyclic voltammetric (CV) investigations were performed to study the electrochemical activity of the GE and NiO-GE electrodes. The CV responses for 0 ppb (absence of As^{3+}) and 5 ppb arsenic (As^{3+}) were recorded using GE and NiO-GE as working electrodes under the three-electrode assembly. The obtained CV of GE exhibits a very low current response compared to the NiO-GE for 0 ppb As^{3+} (Figure 4a). The recorded CV responses of the GE and NiO-GE for 5 ppb As^{3+} in the applied potential window of 0–1.0 V at a scan rate of 50 mVs^{-1} are shown in Figure 4b. The CV response of GE showed a lower current response for the electro-oxidation of 5 ppb As^{3+} at $\sim 0.3 \text{ V}$.

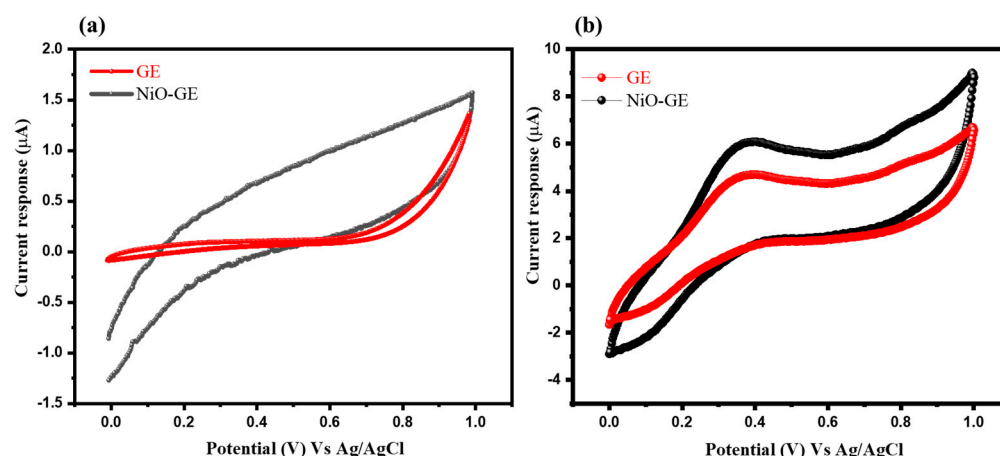


Figure 4. CV responses of GE and NiO-GE for 0 ppb (a) and 5 ppb As^{3+} (b) in 0.1 M PBS (pH = 6) at scan rate = 50 mVs^{-1} .

In contrast, an enhanced current response was observed for NiO-GE for the electro-oxidation of 5 ppb arsenic at $\sim 0.3 \text{ V}$ under the same conditions. This CV study clearly reveals that NiO-GE, relatively speaking, has much better electro-catalytic properties for the sensing of As^{3+} compared to those of GE (Figure 4b). Further investigations were

also performed using the CV method and various amounts of As^{3+} were used. The CV response of the NiO-GE was recorded for various concentrations of As^{3+} in the range of 5–50 ppb. The collected CV responses of NiO-GE for various concentrations of As^{3+} in the range of 5–50 ppb at a scan rate of 50 mVs^{-1} are provided in Figure 5a. According to Figure 5a, it can be observed that the current response for NiO-GE increased with the increase in the concentration of As^{3+} . Thus, we can say that the current response of the NiO-GE may be directly proportional to the concentration of As^{3+} . To examine the linearity of the current response, we have plotted the linear calibration curve of the current response against the concentration of As^{3+} . The observations revealed that the current response increases linearly with the increasing concentration of As^{3+} (Figure 5b).

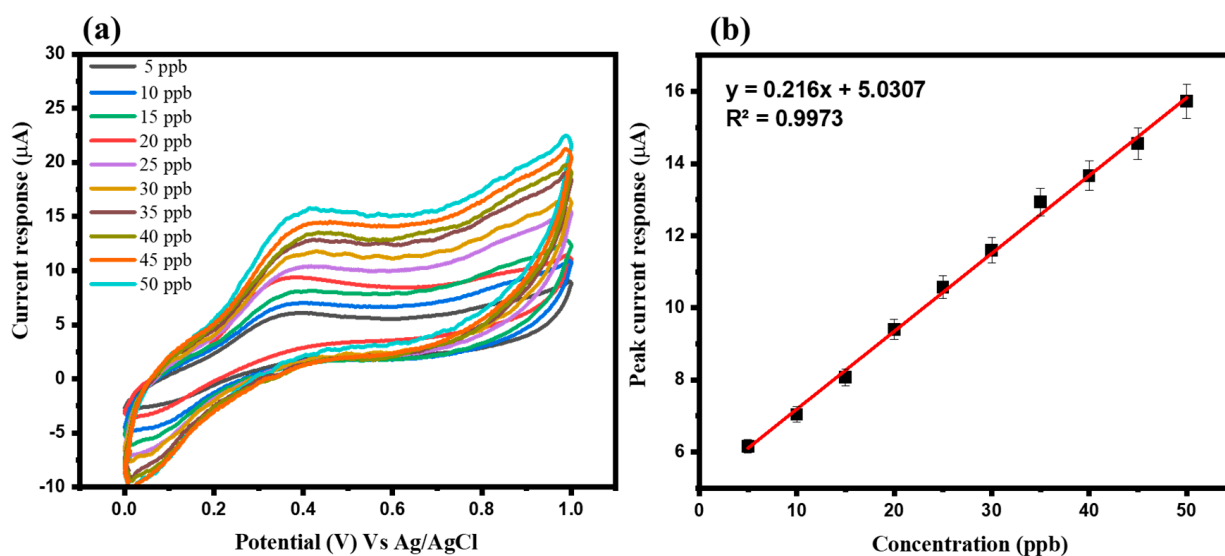


Figure 5. (a) CV response and (b) calibration plot of the NiO-GE with respect to concentration of As^{3+} (0.1 M PBS of pH = 6) at scan rate = 50 mVs^{-1} .

The scan rate used for the CV measurements also plays a vital role and can affect the potential or current responses of the constructed sensors. Thus, various scan rates of $50\text{--}500 \text{ mVs}^{-1}$ were used for further CV measurements of NiO-GE for 5 ppb As^{3+} . The CV response of NiO-GE was obtained for 5 ppb As^{3+} at various applied scan rates in the range of $50\text{--}500 \text{ mVs}^{-1}$. The obtained CV responses of NiO-GE for 5 ppb As^{3+} at various applied scan rates are summarized in Figure 6a. The observed results clearly show that the current response for the detection of 5 ppb As^{3+} increased upon changing the scan rate from 50 to 500 mVs^{-1} . It is clear that the current response of the NiO-GE for 5 ppb As^{3+} increased with respect to the applied scan rate. The plotted calibration curve of the NiO-GE between the peak current response and the applied scan rates is shown in Figure 6b. The increased current response was found to be linear (Figure 6b).

The CV responses of the GE and NiO-GE for 0 ppb As^{3+} (absence of As^{3+}) were also obtained at various scan rates ($50\text{--}500 \text{ mVs}^{-1}$). The CV responses of the GE and NiO-GE increased with increasing scan rate, as shown in Figure 6c,d. However, no oxidation peak was observed due to the absence of As^{3+} .

The repeatability for 5 ppb As^{3+} was also studied by obtaining the CV response of NiO-GE at a scan rate of 50 mVs^{-1} . The obtained 1st, 20th, and 50th CV graphs of NiO-GE for 5 ppb As^{3+} at scan rate of 50 mVs^{-1} are presented in Figure 7.

There was a small degradation in current response observed, which can be neglected. These results suggest good repeatability of NiO-GE for 5 ppb As^{3+} . We can also say that NiO-GE is stable up to 50 cycles (Figure 7). Selectivity is a major challenge for any sensor to be used in practical applications. Previous studies also emphasized the investigation of the selective nature of As^{3+} sensors. Thus, our research group also examined the selectivity of the NiO-GE for the detection of 5 ppb As^{3+} . The CV response of NiO-GE for 5 ppb As^{3+}

was recorded at a scan rate of 50 mVs^{-1} . The CV response of the NiO-GE was also recorded for 5 ppb As^{3+} + 30 ppb interferences (Cd^{2+} , Hg^{2+} , Cu^{2+} , Zn^{2+} , Mg^{2+} , and Pb^{2+}) under the same scan rate.

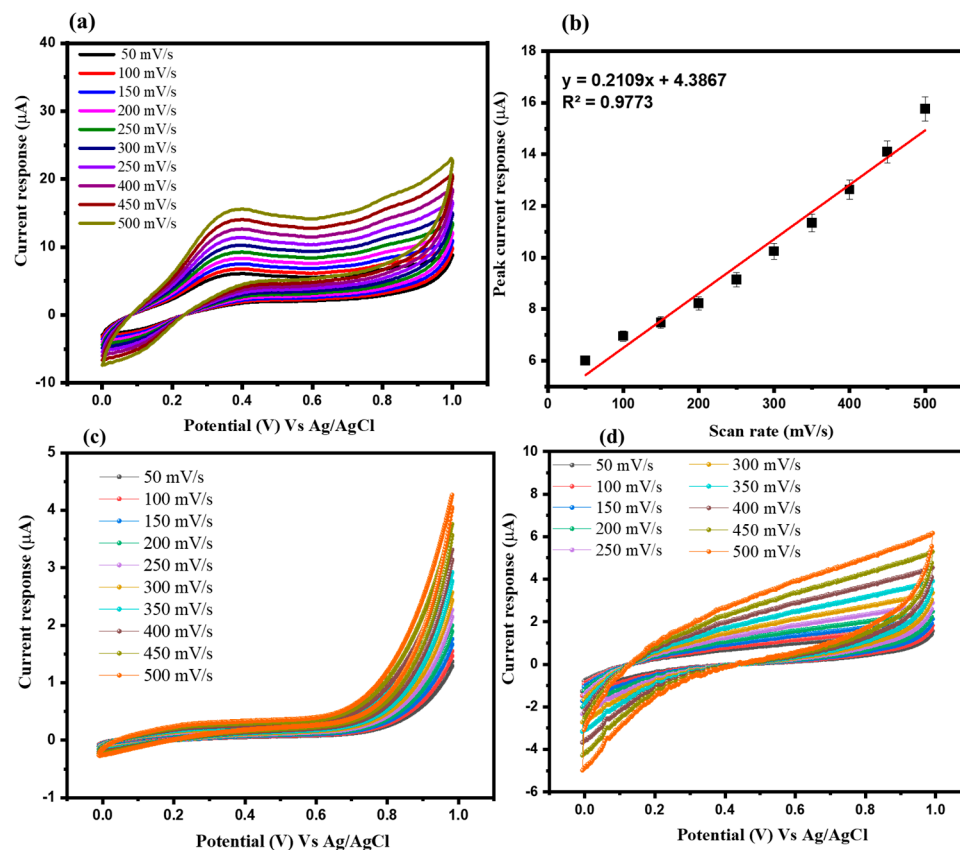


Figure 6. (a) CV response and (b) calibration plot of the NiO-GE for 5 ppb As^{3+} (0.1 M PBS of pH = 6) with respect to the scan rates (50–500 mVs^{-1}). CV responses of GE (c) and NiO-GE (d) for 0 ppb As^{3+} at various scan rates (50–500 mVs^{-1}).

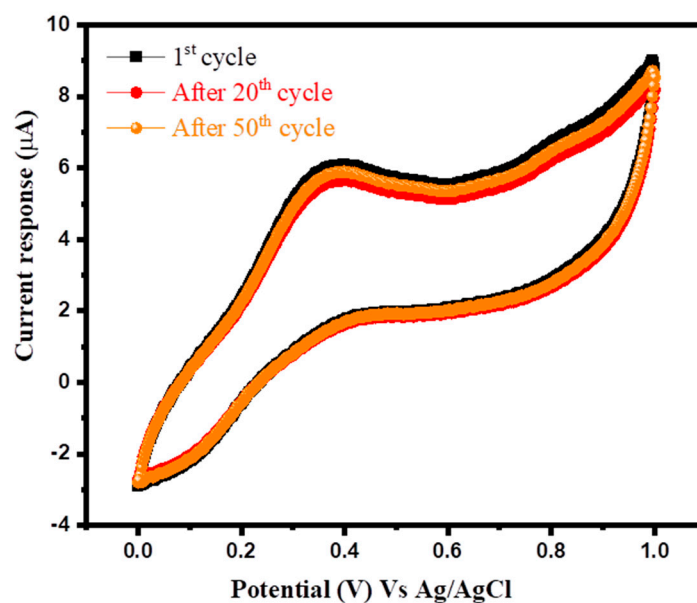


Figure 7. CV responses (1st, 20th, and 50th) of NiO-GE for 5 ppb As^{3+} (0.1 M PBS of pH = 6) at scan rate = 50 mVs^{-1} .

The obtained results are shown in Figure 8. It can be seen that presence of interferences (Cd^{2+} , Hg^{2+} , Cu^{2+} , Zn^{2+} , Mg^{2+} , and Pb^{2+}) even with relatively a high concentration could not change the current of NiO-GE for As^{3+} (Figure 8). This shows that NiO-GE has good selective nature for the determination As^{3+} . We have also obtained the CV graph of NiO-GE in the absence of As^{3+} but in the presence of interferences. The observations showed that NiO-GE has a good selective nature in the presence of interferences (Figure 8).

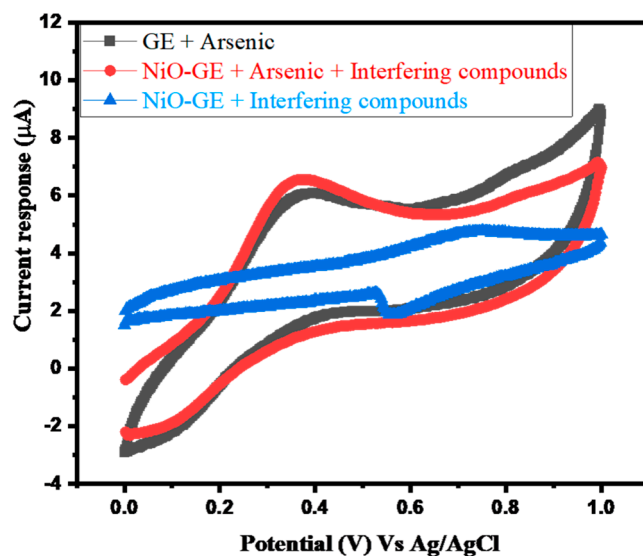


Figure 8. CV response of NiO-GE for 5 ppb As^{3+} only (black) and 5 ppb As^{3+} + 30 ppb interferences (Cd^{2+} , Hg^{2+} , Cu^{2+} , Zn^{2+} , Mg^{2+} , and Pb^{2+}) (0.1 M PBS of pH = 6) at scan rate = 50 mVs^{-1} (red). CV response of NiO-GE for 0 ppb As^{3+} + 30 ppb interferences (Cd^{2+} , Hg^{2+} , Cu^{2+} , Zn^{2+} , Mg^{2+} , and Pb^{2+}) (0.1 M PBS of pH = 6) at scan rate = 50 mVs^{-1} (blue).

Further sensing investigations were performed via linear sweep voltammetry (LSV). The LSV studies were conducted with a three-electrode system. The LSV responses of the GE and NiO-GE for 5 ppb As^{3+} were obtained. The collected LSV responses of the GE and NiO-GE for 5 ppb As^{3+} in the applied potential window of 0–1.0 V at a scan rate of 50 mVs^{-1} are presented in Figure 9. The LSV response of GE exhibits a poor current response for 5 ppb arsenic, whereas an improved current response was observed for NiO-GE (Figure 9).

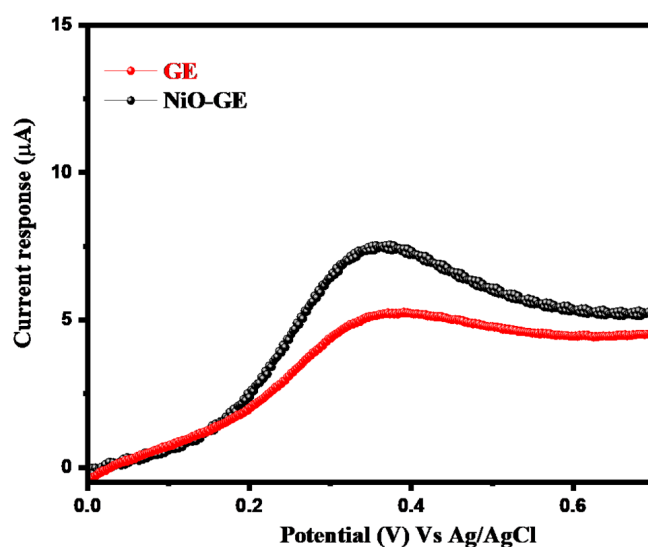


Figure 9. LSV response of GE and NiO-GE for 5 ppb As^{3+} (0.1 M PBS of pH = 6) at scan rate = 50 mVs^{-1} .

The obtained LSV responses show a similar trend as that observed for the CV study. Subsequently, we have obtained LSVV responses for NiO-GE at various concentrations of As^{3+} at a scan rate of 50 mVs^{-1} . The recorded LSV responses for NiO-GE at various concentrations of As^{3+} of 5–50 ppb are summarized in Figure 10a. Figure 10a shows that the current response for NiO-GE slowly increased with the increasing concentration of As^{3+} . Therefore, it can be said that the current response of the NiO-GE may be directly proportional to the concentration of As^{3+} . We have plotted a linear calibration curve of the current response against the concentration of As^{3+} and presented it in Figure 10b.

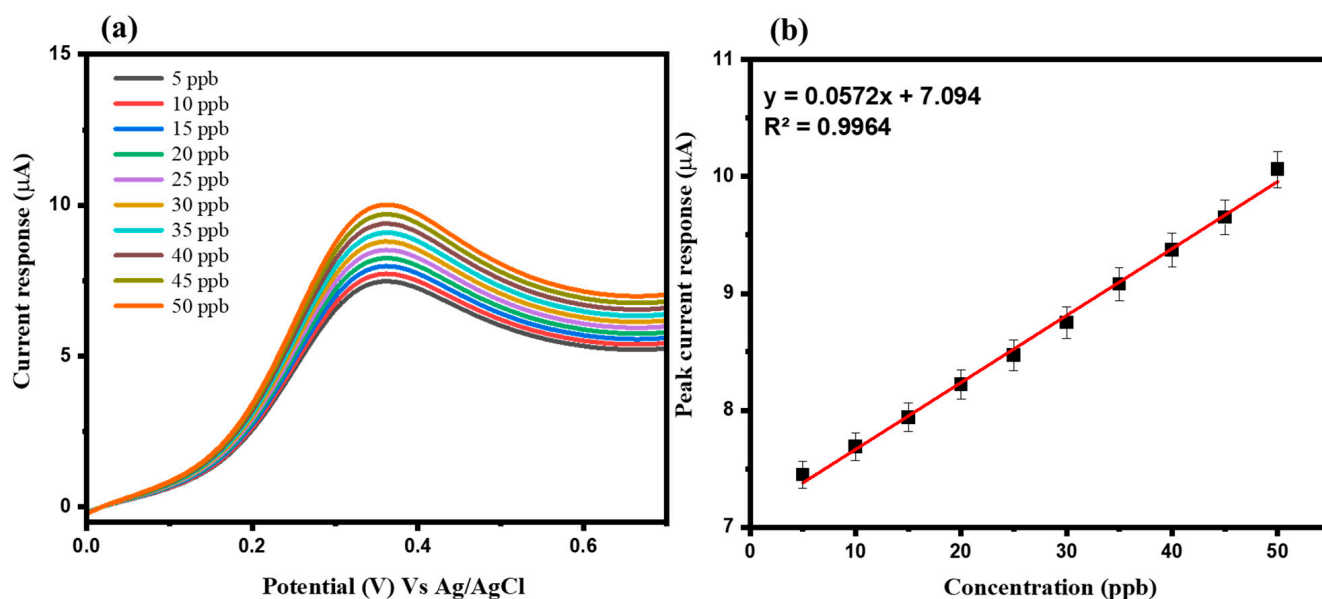


Figure 10. (a) LSV response and (b) calibration plot of the NiO-GE with respect to concentration of As^{3+} (0.1 M PBS of pH = 6) at scan rate = 50 mVs^{-1} .

The observations showed that the current response of NiO-GE increases linearly with the increasing concentration of As^{3+} (Figure 10b).

The repeatability for 5 ppb As^{3+} was also studied by obtaining the LSV response of NiO-GE at a scan rate of 50 mVs^{-1} . The obtained 1st, 20th, and 50th LSV curves of NiO-GE for 5 ppb As^{3+} are shown in Figure 11. From the observed results it can be seen that a small degradation/variation in the current response appeared, which can be neglected. This suggests good repeatability and stability of NiO-GE for 5 ppb As^{3+} (Figure 11) up to 50 cycles.

We have also explored the LSV technique to further examine the selectivity of the NiO-GE for As^{3+} detection. The obtained LSV responses of the NiO-GE for 5 ppb As^{3+} and 5 ppb As^{3+} + 30 ppb interferences (Cd^{2+} , Hg^{2+} , Cu^{2+} , Zn^{2+} , Mg^{2+} , and Pb^{2+}) at a scan rate of 50 mVs^{-1} are provided in Figure 12. From Figure 12, it can be seen that interferences (Cd^{2+} , Hg^{2+} , Cu^{2+} , Zn^{2+} , Mg^{2+} , and Pb^{2+}) at almost six times the concentration do not change the current of NiO-GE for As^{3+} (Figure 12). This can be summarized as NiO-GE having a good selective nature for the determination of As^{3+} . The probable sensing mechanism for the detection of As^{3+} has been described in Scheme 2. The electro-oxidation of As^{3+} takes place at the NiO-GE surface. This process involves the release of two electrons and is expected to be an irreversible process. The electro-oxidation of As^{3+} formed As^{5+} , as shown in Scheme 2.

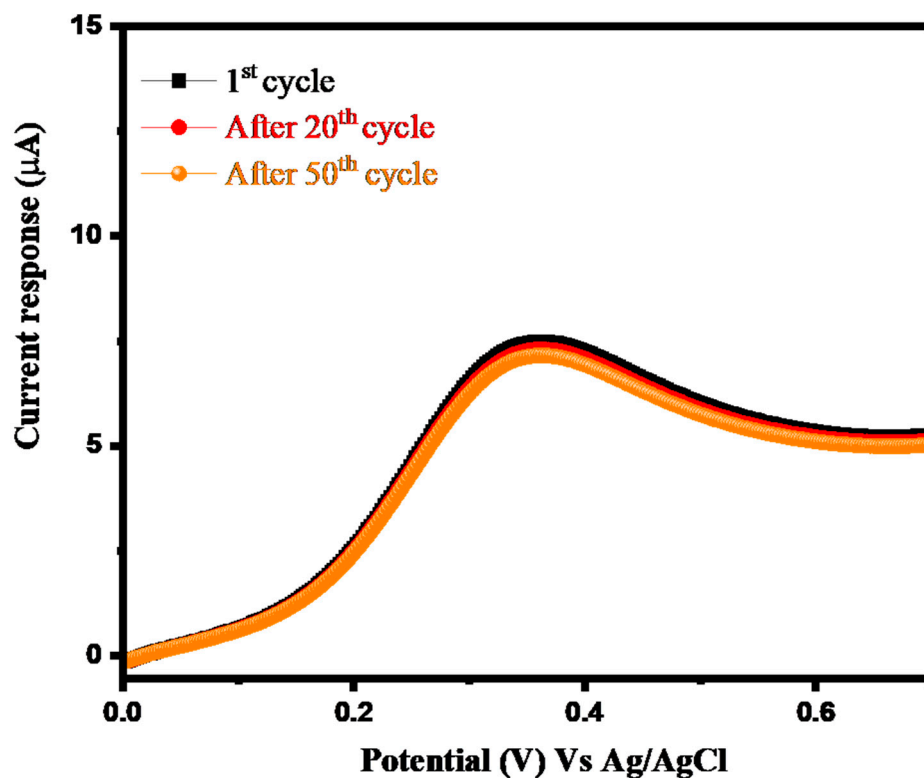


Figure 11. LSV responses (1st, 20th, and 50th) of NiO-GE for 5 ppb As^{3+} (0.1 M PBS of pH = 6) at scan rate = 50 mVs^{-1} .

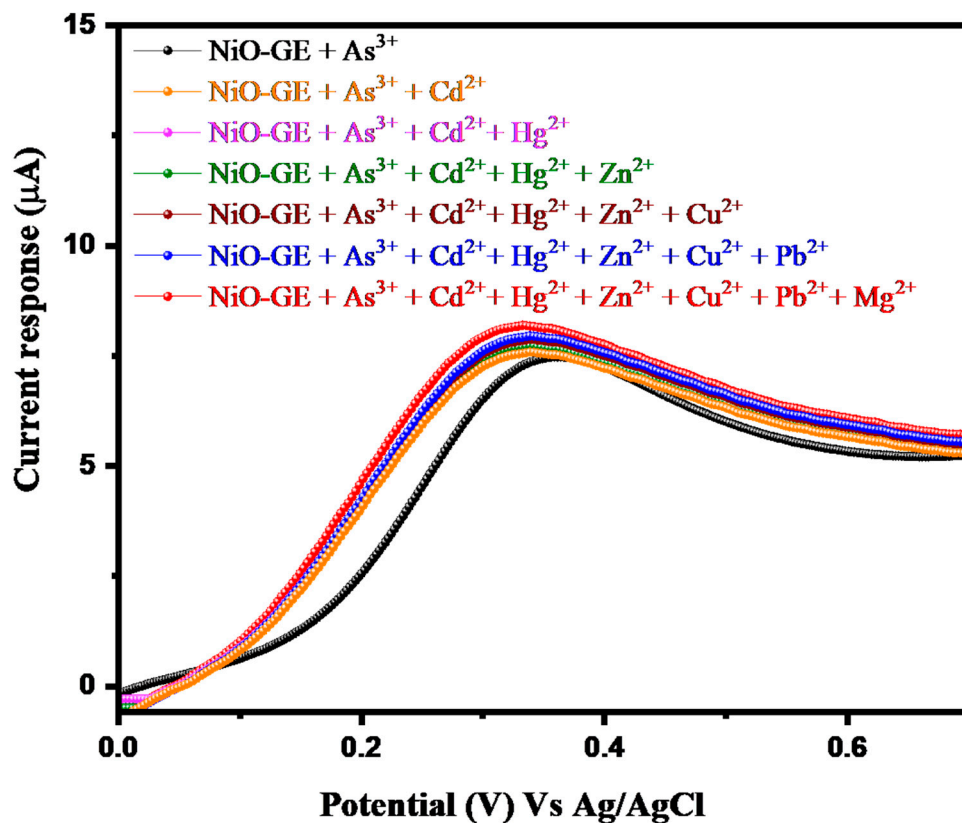


Figure 12. LSV response of NiO-GE for 5 ppb As^{3+} and 5 ppb As^{3+} + 30 ppb interferences (Cd^{2+} , Hg^{2+} , Cu^{2+} , Zn^{2+} , Mg^{2+} , and Pb^{2+}) (0.1 M PBS of pH = 6) at scan rate = 50 mVs^{-1} .

The limit of detection and sensitivity were calculated according to previous reports using the formulas $LOD = 3.3(\sigma/S)$ (where σ is the standard error and S is the slope of the calibration curve) and $sensitivity = slope/area$ of the electrode.

The obtained LoD and sensitivity of NiO for As^{3+} detection are presented in Table 1 and compared with previous reports.

In the previous years, various arsenic sensors have been reported. In this vein, a gold(Au)/manganese oxide (α - MnO_2) electro-catalyst was reported as an arsenic-sensing material which showed a good LOD of 0.019 ppb, including a decent sensitivity of $0.828 \mu\text{Appb}^{-1}$ [38]. AuNPs/nafion was also used as a suitable electrode material and an interesting LOD of 0.047 ppb was achieved [39]. A cobalt-based oxide-modified GCE (CoO_x /GCE) was adopted as an arsenic sensor by Salimi et al. [40] and LOD of 0.83 ppb was obtained. Similarly, a GCE modified with Au/carbon nanotubes (CNTs) was explored as an arsenic sensor, demonstrating LOD of 0.1 ppb [41]. Zirconium oxide (ZrO_2) has been used as an arsenic-sensing material by Bhanjana et al. [24] and a mercaptoethylamine/Au-based arsenic sensor was reported by Li et al. [42]. These reported sensors demonstrated good sensing performance in terms of LOD. Furthermore, tin oxide (SnO) and an iron-based oxide (Fe_3O_4)/reduced graphene oxide (rGO) composite were reported as arsenic-sensing materials which exhibited good LOD [43,44]. In other reports, MnO_x /Au, CoO, manganese ferrite ($MnFe_2O_4$), and AuNPs/cerium oxide (CeO_2)- ZrO_2 were also used as arsenic-sensing materials and reasonable LOD values were reported [45–48]. A graphene/lead oxide (PbO_2)-based arsenic sensor showed LOD of 0.01 ppb and a Au NP/polyaniline-based sensor exhibited LOD of 0.4 ppb [49,50]. In the present work, we have obtained an interesting LOD of 1.94 ppb and a sensitivity of $3.10 \mu\text{Appb}^{-1}$. The obtained sensitivity in our work is higher compared to other reports, as shown in Table 1 [24,38–57].

Table 1. Comparison of performance of NiO-GE with previous sensors.

Materials	LOD (ppb)	Sensitivity (μAppb^{-1})	Dynamic Linear Range (ppb)	References
Au/ α - MnO_2	0.019	0.828	1–10	[46]
Au NPs/nafion	0.047	-	0.1–12	[47]
CoO_x /GCE	0.83	0.11	15–300	[48]
Au/CNTs/GCE	0.1	0.00075	0.75–7.5	[49]
ZrO_2	5	-	5–60	[24]
Mercaptoethylamine/Au	0.02	-	0.2–300	[50]
SnO_2	10	-	-	[51]
Fe_3O_4 /rGO	0.38	-	-	[52]
MnO_x /Au NP	0.057	-	-	[53]
$MnFe_2O_4$	3.37	-	-	[54]
AuNPs/ CeO_2 - ZrO_2	0.137	-	-	[55]
Graphene/ PbO_2	0.01	-	-	[56]
Au NP/polyaniline	0.4	-	-	[57]
NiO-GE	1.94	3.10	5–50	This work

4. Conclusions

In conclusion, we can finally state that the sol-gel synthetic approach has been adopted to obtain nickel oxide (NiO) nanoparticles. The obtained NiO nanoparticles show good electro-catalytic properties and an arsenic sensor has been constructed. A gold (Au) electrode (labelled as GE) was used to for the construction of the arsenic sensor. The active surface with a 3 mm diameter was modified with the obtained NiO nanoparticles via a facile drop-casting modification method. This GE electrode modified with NiO nanoparticles (NiO-GE) was further characterized by CV and LSV approaches. This modified electrode

(NiO-GE) has superior sensing performance compared to the non-modified GE (bare GE) and a reasonably good limit of detection of 1.94 ppb; a sensitivity of $3.10 \mu\text{Appb}^{-1}$ and a linear dynamic range of 5–50 ppb were also achieved. The NiO-GE also demonstrated good selectivity and repeatability of 50 cycles via the LSV approach.

Author Contributions: Conceptualization, A.A. and H.A.; methodology, H.A.; validation, A.A. formal analysis, M.F.A.; investigation, M.F.A. and G.M.A.; resources, A.A.; writing—original draft preparation, R.A.K. and A.A.A.; writing—review and editing, A.A. and R.A.K.; supervision, A.A.; funding acquisition, A.A. All authors have read and agreed to the published version of the manuscript.

Funding: This study was funded by Deputyship for Research & Innovation, Ministry of Education in Saudi Arabia for funding this research work through the project no. IFKSURG-2-1607.

Data Availability Statement: Not applicable.

Conflicts of Interest: The authors declare no conflict of interest.

References

1. Ahmad, K.; Mobin, S.M. Recent Progress and Challenges in $\text{A}_3\text{Sb}_2\text{X}_9$ -Based Perovskite Solar Cells. *ACS Omega* **2020**, *5*, 28404–28412. [[CrossRef](#)] [[PubMed](#)]
2. Kumar, P.; Ahmad, K.; Dagar, J.; Unger, E.; Mobin, S.M. Two-Step Deposition Approach for Lead Free $(\text{NH}_4)_3\text{Sb}_2\text{I}_9$ Perovskite Solar Cells with Enhanced Open Circuit Voltage and Performance. *ChemElectroChem* **2021**, *8*, 3150–3154. [[CrossRef](#)]
3. Ahmad, K.; Kumar, P.K.; Mobin, S.M. Hydrothermally Grown SnO_2 Flowers as Efficient Electrode Modifier for Simultaneous Detection of Catechol and Hydroquinone. *J. Electrochem. Soc.* **2019**, *166*, B1577. [[CrossRef](#)]
4. Mandal, B.K.; Suzuki, K.T. Arsenic round the world: A review. *Talanta* **2002**, *58*, 201–235. [[CrossRef](#)] [[PubMed](#)]
5. Zakharova, E.A.; Noskova, G.N.; Antonova, S.G.; Kabakaev, A.S. Speciation of arsenic(III) and arsenic(V) by manganese-mediated stripping voltammetry at gold microelectrode ensemble in neutral and basic medium. *Int. J. Environ. Anal. Chem.* **2014**, *94*, 1478–1498. [[CrossRef](#)]
6. Jiang, J.; Holm, N.; O'Brien, K. Improved Anodic Stripping Voltammetric Detection of Arsenic(III) Using Nanoporous Gold Microelectrode. *ECSS J. Solid State Sci. Technol.* **2015**, *4*, S3024–S3029. [[CrossRef](#)]
7. Korolczuk, M.; Ochab, M.; Rutyna, I. Determination of As(III) by anodic stripping voltammetry following double deposition and stripping steps at two gold working electrodes. *Talanta* **2015**, *144*, 517–521. [[CrossRef](#)]
8. Babar, N.-U.-A.; Joya, K.S.; Tayyab, M.A.; Ashiq, M.N.; Sohail, M. Highly Sensitive and Selective Detection of Arsenic Using Electrogenated Nanotextured Gold Assemblage. *ACS Omega* **2019**, *4*, 13645–13657. [[CrossRef](#)]
9. Majid, E.; Hrapovic, S.; Liu, Y.L.; Male, K.B.; Luong, J.H.T. Electrochemical determination of arsenite using a gold nanoparticle modified glassy carbon electrode and flow analysis. *Anal. Chem.* **2006**, *78*, 762–769. [[CrossRef](#)]
10. Hassan, S.S.; Sirajuddin; Solangi, A.R.; Kazi, T.G.; Kalhor, M.S.; Junejo, Y.; Tagar, Z.A.; Kalwar, N.H. Nafion stabilized ibuprofen-gold nanostructures modified screen printed electrode as arsenic(III) sensor. *J. Electroanal. Chem.* **2012**, *682*, 77–82. [[CrossRef](#)]
11. Lu, D.; Sullivan, C.; Brack, E.M.; Drew, C.P.; Kurup, P. Simultaneous voltammetric detection of cadmium(II), arsenic(III), and selenium(IV) using gold nanostar-modified screen-printed carbon electrodes and modified Britton-Robinson buffer. *Anal. Bioanal. Chem.* **2020**, *412*, 4113–4125. [[CrossRef](#)] [[PubMed](#)]
12. Wu, J.; Yang, M.; Xiao, J.; Fu, X.; Jin, J.; Li, L.; Chang, W.; Xie, C. Gold Nanoparticle Dropped Titania Microsphere Hybrids as an Enhanced Sensitive Material for Stripping Voltammetry Determination of As(III). *J. Electrochem. Soc.* **2013**, *160*, B225–B230. [[CrossRef](#)]
13. Kato, D.; Kamata, T.; Kato, D.; Yanagisawa, H.; Niwa, O. Au Nanoparticle-Embedded Carbon Films for Electrochemical As^{3+} Detection with High Sensitivity and Stability. *Anal. Chem.* **2016**, *88*, 2944–2951. [[CrossRef](#)] [[PubMed](#)]
14. Yang, M.; Chen, X.; Liu, J.-H.; Huang, X.-J. Enhanced anti-interference on electrochemical detection of arsenite with nanoporous gold in mild condition. *Sens. Actuators B Chem.* **2016**, *234*, 404–411. [[CrossRef](#)]
15. Sahoo, S.; Sahoo, P.K.; Satpati, A.K. Gold Nano Particle and Reduced Graphene Oxide Composite Modified Carbon Paste Electrode for the Ultra Trace Detection of Arsenic (III). *Electroanalysis* **2017**, *29*, 1400–1409. [[CrossRef](#)]
16. Rani, S.; Das, R.K.; Jaiswal, A.; Singh, G.P.; Palwe, A.; Saxena, S.; Shukla, S. 4D nanoprinted sensor for facile organo-arsenic detection: A two-photon lithography-based approach. *Chem. Eng. J.* **2023**, *454*, 140130. [[CrossRef](#)]
17. Wang, W.; Bao, N.; Yuan, W.; Si, N.; Bai, H.; Li, H.; Zhang, Q. Simultaneous determination of lead, arsenic, and mercury in cosmetics using a plastic based disposable electrochemical sensor. *Microchem. J.* **2019**, *148*, 240–247. [[CrossRef](#)]
18. Sullivan, C.; Lu, D.; Brack, E.; Drew, C.; Kurup, P. Voltammetric codetection of arsenic(III) and copper(II) in alkaline buffering system with gold nanostar modified electrodes. *Anal. Chim. Acta* **2020**, *1107*, 63–73. [[CrossRef](#)] [[PubMed](#)]
19. Liebana, S.; Drago, G.A. Bioconjugation and stabilisation of biomolecules in biosensors. *Essays Biochem.* **2016**, *60*, 59–68.
20. Dar, R.A.; Khare, N.G.; Cole, D.P.; Karna, S.P.; Srivastava, A.K. Green synthesis of a silver nanoparticle-graphene oxide composite and its application for As(III) detection. *RSC Adv.* **2014**, *4*, 14432–14440. [[CrossRef](#)]

21. Salimi, A.; Hyde, M.E.; Banks, C.E.; Compton, R.G. Boron doped diamond electrode modified with iridium oxide for amperometric detection of ultra trace amounts of arsenic(III). *Analyst* **2004**, *129*, 9–14. [[CrossRef](#)]
22. Yang, M.; Guo, Z.; Li, L.-N.; Huang, Y.-Y.; Liu, J.-H.; Zhou, Q.; Chen, X.; Huang, X.-J. Electrochemical determination of arsenic(III) with ultra-high anti-interference performance using Au-Cu bimetallic nanoparticles. *Sens. Actuators B Chem.* **2016**, *231*, 70–78. [[CrossRef](#)]
23. Bansod, B.; Kumar, T.; Thakur, R.; Rana, S.; Singh, I. A review on various electrochemical techniques for heavy metal ions detection with different sensing platforms. *Biosens. Bioelectron.* **2017**, *94*, 443–455. [[CrossRef](#)] [[PubMed](#)]
24. Bhanjana, G.; Dilbaghi, N.; Chaudhary, S.; Kim, K.-H.; Kumar, S. Robust and Direct Electrochemical Sensing of Arsenic Using Zirconia Nanocubes. *Analyst* **2016**, *141*, 4211–4218. [[CrossRef](#)] [[PubMed](#)]
25. Hu, H.; Xie, B.; Lu, Y.; Zhu, J. Advances in Electrochemical Detection Electrodes for As(III). *Nanomaterials* **2022**, *12*, 781. [[CrossRef](#)] [[PubMed](#)]
26. Ahmad, K.; Mohammad, A.; Ansari, S.N.; Mobin, S.M. Construction of Graphene Oxide Sheets Based Modified Glassy Carbon Electrode (GO/GCE) for the Highly Sensitive Detection of Nitrobenzene. *Mater. Res. Express* **2018**, *5*, 075601. [[CrossRef](#)]
27. Ahmad, K.; Mobin, S.M. Shape Controlled Synthesis of High Surface Area MgO Microstructures for Highly Efficient Congo Red Dye Removal and Peroxide Sensor. *J. Environ. Chem. Eng.* **2019**, *7*, 103347. [[CrossRef](#)]
28. Ahmad, K.; Mobin, S.M. Design and Fabrication of Cost-Effective and Sensitive Non-Enzymatic Hydrogen Peroxide Sensor Using Co-Doped δ -MnO₂ Flowers as Electrode Modifier. *Anal. Bioanal. Chem.* **2021**, *413*, 789–798. [[CrossRef](#)]
29. Ahmad, K.; Kumar, P.; Mobin, S.M. Hydrothermally Grown Novel Pyramids of the CaTiO₃ Perovskite as an Efficient Electrode Modifier for Sensing Applications. *Mater. Adv.* **2020**, *1*, 2003–2009. [[CrossRef](#)]
30. Ahmad, K.; Mobin, S.M. Construction of Polyaniline/ITO Electrode for Electrochemical Sensor Applications. *Mater. Res. Express* **2019**, *6*, 085508. [[CrossRef](#)]
31. Mobili, R.; Preda, G.; Cognata, S.L.; Toma, L.; Pasini, D.; Amendola, V. Chiroptical sensing of perrhenate in aqueous media by a chiral organic cage. *Chem. Commun.* **2022**, *58*, 3897–3900. [[CrossRef](#)] [[PubMed](#)]
32. You, L.; Zha, D.; Anslyn, E.V. Recent Advances in Supramolecular Analytical Chemistry Using Optical Sensing. *Chem. Rev.* **2015**, *115*, 7840–7892. [[CrossRef](#)] [[PubMed](#)]
33. Benedini, S.; Zheng, Y.; Nitti, A.; Mazza, M.M.A.; Dondi, D.; Raymob, F.M.; Pasini, D. Large polarization of push–pull “Cruciforms” via coordination with lanthanide ions. *New J. Chem.* **2022**, *46*, 221–227. [[CrossRef](#)]
34. Dan-dan, Y.; Yong, Z.; Hong-quan, Y.; Hong, Z. Low temperature synthesis of NiO/CoO nanostructures to enhance their low temperature oxygen reduction catalysis. *Micron* **2022**, *161*, 103326. [[CrossRef](#)] [[PubMed](#)]
35. Hosseinzade, M.R.; Naji, L.; Hasannezhad, F. Electrochemical deposition of NiO bunsenite nanostructures with different morphologies as the hole transport layer in polymer solar cells. *J. Electroanal. Chem.* **2022**, *926*, 116955. [[CrossRef](#)]
36. Kumar, V.M.; Polaki, S.R.; Krishnan, R.; Sarguna, R.M.; Mathews, T. Binder-free vertical graphene nanosheets templated NiO petals for high-performance supercapacitor applications. *J. Alloys Compd.* **2023**, *931*, 167420. [[CrossRef](#)]
37. Mishra, S.; Yogi, P.; Sagdeo, P.R.; Kumar, R. Mesoporous Nickel Oxide (NiO) Nanopetals for Ultrasensitive Glucose Sensing. *Nanoscale Res. Lett.* **2018**, *13*, 16. [[CrossRef](#)]
38. Tyagi, M.; Tomar, M.; Gupta, V. NiO nanoparticle-based urea biosensor. *Biosens. Bioelectron.* **2013**, *41*, 110–115. [[CrossRef](#)]
39. Jahani, P.M.; Javar, H.A.; Mahmoudi-Moghaddam, H. A new electrochemical sensor based on Europium-doped NiO nanocomposite for detection of venlafaxine. *Measurement* **2021**, *173*, 108616. [[CrossRef](#)]
40. Amin, S.; Tahira, A.; Solangi, A.; Mazzaro, R.; Ibupoto, Z.H.; Vomiero, A. A sensitive enzyme-free lactic acid sensor based on NiO nanoparticles for practical applications. *Anal. Methods* **2019**, *11*, 3578–3583. [[CrossRef](#)]
41. Bakhsh, H.; Buledi, J.A.; Khand, N.H.; Junejo, B.; Solangi, A.R.; Mallah, A.; Sherazi, S.T.H. NiO nanostructures based functional none-enzymatic electrochemical sensor for ultrasensitive determination of endosulfan in vegetables. *Food Meas.* **2021**, *15*, 2695–2704. [[CrossRef](#)]
42. Jahromi, S.P.; Pandikumar, A.; Goh, B.T.; Lim, Y.S.; Basirun, W.J.; Lim, H.N.; Huang, N.M. Influence of particle size on performance of a nickel oxide nanoparticle-based supercapacitor. *RSC Adv.* **2015**, *5*, 14010–14019. [[CrossRef](#)]
43. Mateos, D.; Valdez, B.; Castillo, J.R.; Nedev, N.; Curiel, M.; Perez, O.; Arias, A.; Tiznado, H. Synthesis of high purity nickel oxide by a modified sol-gel method. *Ceram. Int.* **2019**, *45*, 11403–11407. [[CrossRef](#)]
44. Dharmaraj, N.; Prabu, P.; Nagarajan, S.; Kim, C.H.; Park, J.H.; Kim, H.Y. Synthesis of nickel oxide nanoparticles using nickel acetate and poly(vinyl acetate) precursor. *Mater. Sci. Eng. B* **2006**, *128*, 111–114. [[CrossRef](#)]
45. Jeremić, D.; Andjelković, L.; Milenković, M.R.; Šuljagić, M.; Ristović, M.S.; Ostojić, S.; Nikolić, A.S.; Vulić, P.; Brčeski, I.; Pavlović, V. One-Pot Combustion Synthesis of Nickel Oxide and Hematite: From Simple Coordination Compounds to High Purity Metal Oxide Nanoparticles. *Sci. Sinter.* **2020**, *52*, 481–490. [[CrossRef](#)]
46. Yang, M.; Chen, X.; Jiang, T.-J.; Guo, Z.; Liu, J.-H.; Huang, X.-J. Electrochemical Detection of Trace Arsenic(III) by Nanocomposite of Nanorod-Like α -MnO₂ Decorated with ~5 nm Au Nanoparticles: Considering the Change of Arsenic Speciation. *Anal. Chem.* **2016**, *88*, 9720–9728. [[CrossRef](#)]
47. Huang, J.-F.; Chen, H.-H. Gold-nanoparticle-embedded Nafion Composite Modified on Glassy Carbon Electrode for Highly Selective Detection of Arsenic (III). *Talanta* **2013**, *116*, 852–859. [[CrossRef](#)]
48. Salimi, A.; Mamkhezri, H.; Hallaj, R.; Soltanian, S. Electrochemical Detection of Trace amount of Arsenic(III) at Glassy Carbon Electrode Modified with Cobalt Oxide Nanoparticles. *Sens. Actuators B Chem.* **2008**, *129*, 246. [[CrossRef](#)]

49. Xiao, L.; Wildgoose, G.G.; Compton, R.G. Sensitive Electrochemical Detection of Arsenic (III) using Gold Nanoparticle Modified Carbon Nanotubes via Anodic Stripping Voltammetry. *Anal. Chim. Acta* **2008**, *620*, 44–49. [[CrossRef](#)]
50. Li, D.; Li, J.; Jia, X.; Han, Y.; Wang, E. Electrochemical Determination of Arsenic(III) on Mercaptoethylamine Modified Au Electrode in Neutral Media. *Anal. Chim. Acta* **2012**, *733*, 23–27. [[CrossRef](#)]
51. Bhanjana, G.; Mehta, N.; Chaudhary, G.R.; Dilbaghi, N.; Kim, K.-H.; Kumar, S. Novel electrochemical sensing of arsenic ions using a simple graphite pencil electrode modified with tin oxide nanoneedles. *J. Mol. Liq.* **2018**, *264*, 198–204. [[CrossRef](#)]
52. Agustiany, T.; Khalil, M.; Einaga, Y.; Jiwanti, P.K.; Ivandini, T.A. Stable iridium-modified boron-doped diamond electrode for the application in electrochemical detection of arsenic (III). *Mater. Chem. Phys.* **2020**, *244*, 122723. [[CrossRef](#)]
53. Wu, S.; Zhao, Q.; Zhou, L.; Zhang, Z. Stripping Analysis of Trace Arsenic Based on the MnOx/AuNPs Composite Film Modified Electrode in Alkaline Media. *Electroanalysis* **2014**, *26*, 1840–1849. [[CrossRef](#)]
54. Zhou, S.; Han, X.; Fan, H.; Liu, Y. Electrochemical Sensing toward Trace As(III) Based on Mesoporous MnFe₂O₄/Au Hybrid Nanospheres Modified Glass Carbon Electrode. *Sensors* **2016**, *16*, 935. [[CrossRef](#)]
55. Yang, M.; Li, P.-H.; Xu, W.-H.; Wei, Y.; Li, L.-N.; Huang, Y.-Y.; Sun, Y.-F.; Chen, X.; Liu, J.-H.; Huang, X.-J. Reliable electrochemical sensing arsenic (III) in nearly groundwater pH based on efficient adsorption and excellent electrocatalytic ability of AuNPs/CeO₂-ZrO₂ nanocomposite. *Sens. Actuators B* **2018**, *255*, 226–234. [[CrossRef](#)]
56. Ramesha, G.K.; Sampath, S. In situ formation of graphene–lead oxide composite and its use in trace arsenic detection. *Sens. Actuators B* **2011**, *160*, 306–311. [[CrossRef](#)]
57. Chowdhury, A.-N.; Ferdousi, S.; Islam, M.M.; Okajima, T.; Ohsaka, T. Arsenic detection by nanogold/conductingpolymer-modified glassy carbon electrodes. *J. Appl. Polym. Sci.* **2007**, *104*, 1306–1311. [[CrossRef](#)]

Disclaimer/Publisher’s Note: The statements, opinions and data contained in all publications are solely those of the individual author(s) and contributor(s) and not of MDPI and/or the editor(s). MDPI and/or the editor(s) disclaim responsibility for any injury to people or property resulting from any ideas, methods, instructions or products referred to in the content.